Biosensors and Bioelectronics 25 (2009) 870–876

Contents lists available at ScienceDirect

Biosensors and Bioelectronics

journal homepage: www.elsevier.com/locate/bios

Potential of a simplified measurement scheme and device structure for a low cost label-free point-of-care capacitive biosensor

Elder A. de Vasconcelos[a], Newton G. Peres[b], Cintya O. Pereira[b], Valdinete L. da Silva[c], Eronides F. da Silva Jr.[a], Rosa F. Dutra[b,*]

[a] Departamento de Física, Universidade Federal de Pernambuco, Av. Prof. Moraes Rego, s/n, Cidade Universitária, Recife-PE, Brazil
[b] Laboratório de Pesquisa em Diagnóstico/LAPED, PROCAPE, Universidade de Pernambuco, Rua Arnóbio Marques, Santo Amaro, 310, 50100-130, Recife-PE, Brazil
[c] Departamento de Engenharia Química, Universidade Federal de Pernambuco, Av. Prof. Moraes Rego, s/n, Cidade Universitária, 50740-521, Recife-PE, Brazil

ARTICLE INFO

Article history:
Received 3 June 2009
Received in revised form 13 August 2009
Accepted 28 August 2009
Available online 12 September 2009

Keywords:
Label-free
Point-of-care
Capacitive immunosensor
Troponin
Acute myocardial infarction
Immunoglobulin

ABSTRACT

A simplified measurement scheme and device structure aiming at developing a low cost, label-free, point-of-care capacitive biosensor were investigated. The detection principle is the increase of low frequency capacitance between two planar Al electrodes observed after antibody–antigen interaction. The electrodes, deposited on oxidized Si wafers, were covered with an antibody layer, with and without using self-assembled thiol monolayer. Immunoglobulin G (IgG) and cardiac troponin T (TnT) were used as analytes to asses this proposal. The device was able to detect successfully TnT levels in the range 0.07 to 6.83 ng/mL in human serum from patients with cardiac diseases and in the range 0.01 ng/mL to 5 ng/mL for TnT in phosphate buffer saline. An equivalent circuit model able to reproduce the general behavior of experimental capacitance versus frequency curves was presented. The investigated features that have potential to reduce costs and simplify measurements were: use of single, low frequency (1 kHz) measurement signal, within the range of low cost portable capacitance meters; employment of a lower cost electrode material, aluminum, instead of gold electrodes; and use of simple and miniaturized planar two-electrodes arrangement, thus making a portable system for point-of-care applications.

Published by Elsevier B.V.

1. Introduction

The use of antigen or antibody label conjugate is the most common method to quantify interest analytes employed in clinical and research studies. The utilization of these conjugates does not always express reliable results. Non-specific bindings, interference of samples on markers signals and increased number of steps are related with the decrease of performance of those immunoassays. Therefore, to use label-free detection to circumvent the need to modify biomolecules with fluorescent dyes, enzymes redox or radioactive labels may lead to simplification, speed, reliability and lower cost (Fan et al., 2008).

The design of non-labeled affinity biosensors has been extensively studied in academy and industry. One source of impetus is the demand of point-of-care diagnostics, which requires simple equipment and the potential for label-free analysis. The main technologies of label-free affinity biosensors currently in use or under development are: surface plasmon resonance (SPR) devices, mass-sensitive piezoelectric oscillators, field effect transistor (FET) sensors and electrochemical impedance biosensors.

In SPR systems, affinity binding occurring on metallic surfaces promotes the modification of the SPR minimum, which may be used as a quantification parameter of antigen–antibody reactions (Boozer et al., 2006). Besides label-free detection, its potential to detect molecules less than 0.5 kDa of molecular weight and in concentrations below 10 pg/mm^2 are the most attractive features of this technique (Shiau et al., 2008). However, this system requires more complex and expensive instrumentation than the other label-free sensor technologies (Luppa et al., 2001).

In mass-sensitive piezoelectric oscillators, the detection principle is based on oscillator frequency changes due to affinity binding on the surface of the piezoelectrics. This technology is cheaper than SPR technology. Unfortunately, the oscillator frequency may be also strongly affected by the viscoelastic properties of the immobilized antibodies and non-specific adsorptions in liquid media. Moreover, the high cost of transducers and the difficulty of miniaturization are the main obstacles to the fabrication of low cost and portable equipment (Janshoff and Steinem, 2005).

Recently, label-free detection of different target analytes (proteins, viruses, oligonucleotides) using resistive or FET sensors has attracted much attention due to several demonstrations involv-

* Corresponding author. Tel.: +55 81 3181 7179; fax: +55 81 3183 3302.
E-mail addresses: rfiremandutra@yahoo.com.br, rosa.dutra@pq.cnpq.br (R.F. Dutra).

0956-5663/$ – see front matter. Published by Elsevier B.V.
doi:10.1016/j.bios.2009.08.050

ing the use of nanostructures such as silicon nanowires, carbon nanotubes, porous surfaces and nanoparticles. Nevertheless, the manufacture of FET-based immunoassays imposes rigorous conditions and is expensive (Bangar et al., 2009; Qu et al., 2009).

In impedance biosensors, the detection process usually involves formation of a recognition complex between the sensing biomolecule at the interface of an electronic transducer and the analyte. The interaction between the sensing molecule and the analyte affects the electrical properties of the system. The recognition event can be evaluated by the detection of the overall impedance, or by changes in capacitance or conductance (Khan and Dhayal, 2009). Applications have been demonstrated for various types of analytes, such as antibodies and antigens, nucleic acids, whole cells and microorganisms. Impedance biosensors are now intensively investigated due to their potential for label-free, real-time, in situ detection of various analytes, and the affordability of impedance analyzers and data evaluation software (Yang and Bashir, 2008).

IgG is a glycoprotein (~150 kDa) mainly responsible to combat chronic infectious diseases and for surveillance against recurrence of infections (Janeway et al., 2005), and is a standard model for many immunoassay methods. Cardiac troponins are structural proteins responsible for contractile mechanism in cardiac muscle (Collinson and Gaze, 2005). Currently, the cardiac troponin T isophorm is a "gold-standard" biomarker to identify and to differ cardiac injuries in suspicious patients of acute coronary syndromes (Alpert et al., 2000), as well as to evaluate the damage size in cardiac tissue after myocardial infarction diagnosis (Steen et al., 2006). Intensive care unit and cardiological emergency centers require a high-speed, specific and sensitive assay to quantify TnT levels in the range of sub-ng/mL in serum samples. However, conventional methods, such enzyme-linked immunosorbent assay (ELISA) and electro-chemiluminescence immunossay (ECLIA), for example, are not practical for point-of-care measurements, being time-consuming and requiring several steps and labels.

In this work, we investigated a simple device structure and simplified measurement scheme aiming at developing a low cost, label-free, point-of-care capacitive biosensor. We tested the device successfully with both IgG and TnT analytes.

2. Experimental details

Fig. 1 provides an overview of the device structure and location of the antibody–antigen complex, and also illustrates the detection principle: the low-frequency capacitance increase after antigen–antibody, depicted in Fig. 1III and discussed in detail in Figs. 3 and 4.

2.1. Reagents and samples

Human TnT, lyophilized human troponin T was purchased from Calbiochem and monoclonal goat anti-human TnT (anti-TnT) from Roche Diagnostics (Germany). Goat anti-human IgG, H and L chain specific (anti-IgG), human IgG, 2-aminoethanothiol (cysteamine), 25% glutaraldehyde and glycine were acquired from Sigma–Aldrich (USA). All the other reagents were analytical grade and the solutions used in the experiments were freshly prepared using deionized (DI) water with a resistivity of 18.2 MΩ.cm.

Phosphate buffered saline (PBS), pH 7.4, 10 mM was used in all experiments, except special remark. It was prepared by dissolving 0.2 g KCl, 8.0 g NaCl, 0.24 g KH_2PO_4 and 1.44 g Na_2HPO_4, in 1000 mL of DI water.

Human serum samples of cardiac patients were obtained from the central laboratory of Oswaldo Cruz Hospital (Recife, Brazil). Venous blood was collected and immediately centrifuged for 120 s at 1150 rad/s and TnT was measured using electrochemiluminescence technology (Troponin T STAT, Elecsys 2010, Roche Diagnostic, Germany). All the samples were included in this work after donors or their responsible gave written informed consent.

2.2. Electrical measurements

The devices were positioned on a vacuum chuck, inside a shielded dark box, and contacted by two micromanipulator probes, as shown in Fig. 1I. The probes were connected to a HP 4284A Precision LCR Meter using a 20 mV to 100 mV RMS AC signal from 100 Hz to 1 MHz, without DC bias, with both open and short circuit correction. Repeated scans showed that the relative standard deviation for capacitance measurements was approximately 1.5% for the lowest measurement frequencies (100 Hz to 300 Hz) and below 0.3% for higher frequencies. We defined the relative capacitance variation as

$$\frac{C - C_0}{C_0} \times 100(\%) \quad (1)$$

where C_0 is the capacitance after antibody immobilization and C is the capacitance after exposure to antigen at a particular concentration.

2.3. Device fabrication

Fig. 1II shows the device structure and antibody and antigen locations. The devices were fabricated in a Class 1000 cleanroom (Federal Standard 209D). Si <1 0 0> wafers were cleaned to remove organic and metallic impurities by means of a sequence of 5 min immersions in ultrasonic agitation in high purity chemicals (acetone, methanol and HF, CMOS-grade from J.T. Baker, Inc, USA) with DI water between steps. Immediately after cleaning, the wafers were kept in a 3% HF solution until they were loaded into a tubular furnace to grow a 350 nm-thick, silicon dioxide (SiO_2) layer by wet oxidation. An Al film, 80 nm thick, was thermally evaporated from a tungsten boat onto the SiO_2 layer followed by a 30 min anneal in forming gas at 400 °C. Photolithograph was used to form two Al strips (electrodes) onto the SiO_2 layer, 1.5 mm wide and 2 mm apart. The length of the wafers varied from 7 to 10 mm. The variations, due to the manual process of cutting the wafer into smaller chips, are compensated by our calibration procedure. The response was calibrated by the relative capacitance change, defined in Section 2.2. The device structure after fabrication is shown in Fig. 1II (a).

After device fabrication, the devices were kept in vacuum desiccators until immobilization procedures to avoid organic and inorganic contamination.

2.4. Immobilization procedure

Two biomolecules (anti-IgG and anti-TnT) were immobilized using glutaraldehyde for a covalent binding to amino groups by direct adsorption on the electrode surface and via self-assembled monolayers (SAM), respectively. Fig. 2 shows the sequency of steps in antibodies immobilization that is described in more detail in 2.4.1 and 2.4.2 sessions. A scheme of device structure after antibody immobilization is shown in Fig. 1II(b).

The immobilization procedures involve pipetting the solutions (5 μL) onto the two electrodes. To prevent the evaporation of the biological materials, all the incubations were performed inside a humid environment which consisted of a small petri dish (volume: approximately 12 mL) containing tissue paper soaked with DI water and hermetically sealed with parafilm.

During these procedures of immobilization, gloves and masks were used and caution was exerted to leave uncovered a small area of the electrodes where the probes would make contact.

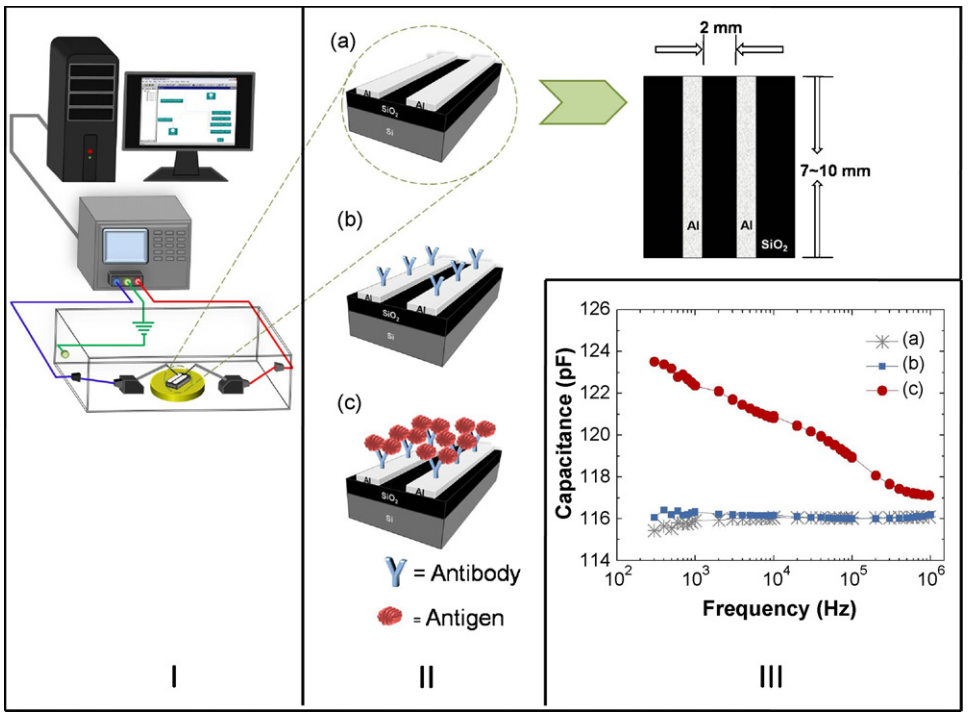

Fig. 1. (I) Measurement setup. (II) Device structure and location of the antibody–antigen complex. (III) Device response to IgG. Capacitance versus frequency characteristics: after device fabrication (a), after anti-IgG immobilization (b), and after pipette dropping of IgG solution onto the electrodes (c).

2.4.1. anti-IgG

First, a mixture of anti-IgG (1.0 μg/mL) + glutaraldehyde (2.5%) (1:1, v/v) was prepared in PBS and left incubating for 45 min. After this, 5 μL of this mixture was spread on the electrodes of Al to form a layer of immobilized anti-IgG. In order to obtain a high degree of surface covering, it is necessary to wait 45 min until the next step, which is to remove the excess of unbound material with two PBS washes followed by rinsing in DI water. The rinsing with DI water is preferred because the ions dispersed in PBS may influence the capacitive response with the variation of capacitance. Finally, a solution of 50 mM glycine in PBS was incubated for 2 h to block non-reactive sites.

2.4.2. anti-TnT

First, the devices were immersed in a solution of 25 mM of 2-aminoethanethiol in ethanol for 2 h. At this stage, a self-assembled monolayer (SAM) layer of thiols is already formed. Afterwards, the excess of unbound material is removed with two ethanol washes. The next step is to prepare a mixture of anti-TnT (1.2 μg/mL) + glutaraldehyde (2.5%) (1:1, v/v) in PBS and left incu-

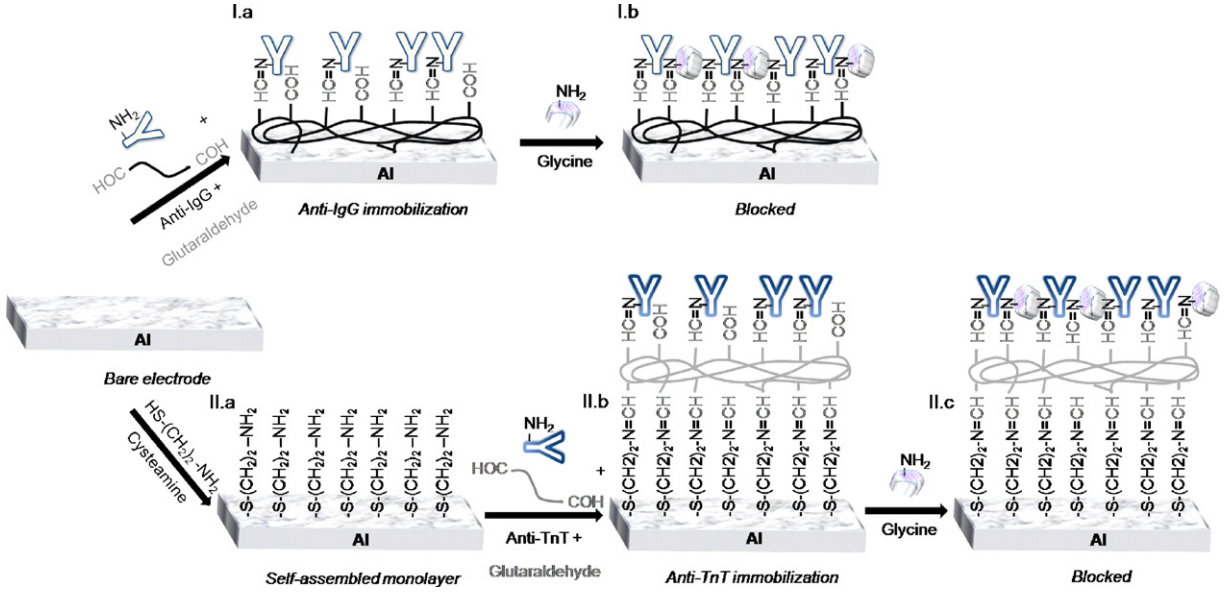

Fig. 2. Sequency of steps of antibodies immobilization on Al electrode: For anti-IgG: Surface is exposed to glutaraldehyde + anti-IgG mixture (I, a); free aldehyde groups are blocked with glycine (I, b). For anti-TnT: self-assembled monolayers of thiol on the Al surface (II, a); aldehyde reacting with amino groups (II, b) and free aldehyde groups are blocked with glycine (II, c).

bating for 1 h so that the anti-TnT amino groups form a crosslink with aldehydes. After incubation, 5 μL of this mixture was spread on the electrodes to promote a covalent bonding with the amino of SAM. Finally, a solution of 50 mM glycine in PBS was incubated for 2 h to block non-reactive sites (Dutra et al., 2007).

2.4.3. Antigen

The antigen solutions (5 μL) were manually pipetted onto the electrodes and left incubating for 30 min. Afterwards, the excess of unbound material is removed with two PBS washes followed by rinsing with DI water. A scheme of the device structure after the antigen–antibody interaction is shown in Fig. 1II (c).

3. Results and discussion

3.1. Immobilization procedures

The fixing of antibodies on the surface and its maintaining over the immunocomplexation is one of the most critical steps in the performance of an immunosensor. There are some techniques to immobilize the antibodies by the F_c region (oriented immobilization), leaving free and far from the support surface the Fab regions: using immobilized protein A or G (Ko et al., 2009), previous site-directed biotinylation of the F_c region to get site direct immobilization on avidin or streptavidin supports (Dutra and Kubota, 2007), and so on. However, these protocols are more or less sophisticated and, in many cases, involve the antibody modification. Other orientations may also have interest and may even be more adequate than these, if the immobilized antibody retains a reasonable percentage of the recognition capacity. Here, we adopted to immobilize the antibodies by Fab regions using the glutaraldehyde to provide a covalent linkage with amino groups very close to the support surface, which permit that antibody capacity to capture antigen are preserved at 65 ± 5% when compared to soluble antibody (Batalla et al., 2008). A two-step immobilization mechanism was adopted, that was, a first anionically exchange of the proteins on the support followed by a supportprotein covalent attachment. In anti-TnT immobilization case, the aminated supports prepared with 2-aminoethanothiol was activated with glutaraldehyde and a further covalent reaction among the nearby residues of the antibodies and the glutaraldehyde groups was performed.

In this study, the thiol-terminated linker, cysteamine, was of short chain length (2 carbons), thus providing higher solubility. Several solvents are used in preparation of self-assembled monolayers, but precaution must be taken because the final composition of the monolayer depends on the relative solubility of the chain length. The incorporation of water free solvents into the assembled monolayer structure increases the repeatability and produces well-ordered monolayers, defected-free SAMs and not-formed multilayers (Liu et al., 2001). Therefore, ethanol was selected as cysteamine solvent instead of water.

3.2. Capacitance analysis

The device capacitance, after fabrication is practically constant in all frequencies, as depicted in Fig. 1III (curve (a)). After antibody immobilization, its value is almost identical to that after fabrication, as shown in Fig. 1III (curve (b)). After antibody–antigen interaction, the device capacitance at low frequencies increases, as shown in Fig. 1III (curve (c)). The data depicted in Fig. 1III are shown again in Fig. 3(a), where it will be discussed in detail. Curves (a), (b) and (c) in Fig. 1III are shown in Fig. 3(a) as curves (1), (2) and (5), respectively.

Fig. 3(a) shows that the device capacitance is slightly affected after repeated procedures of anti-IgG (1 μg/mL) immobilization on the electrodes, whereas it is greatly affected by the deposition of

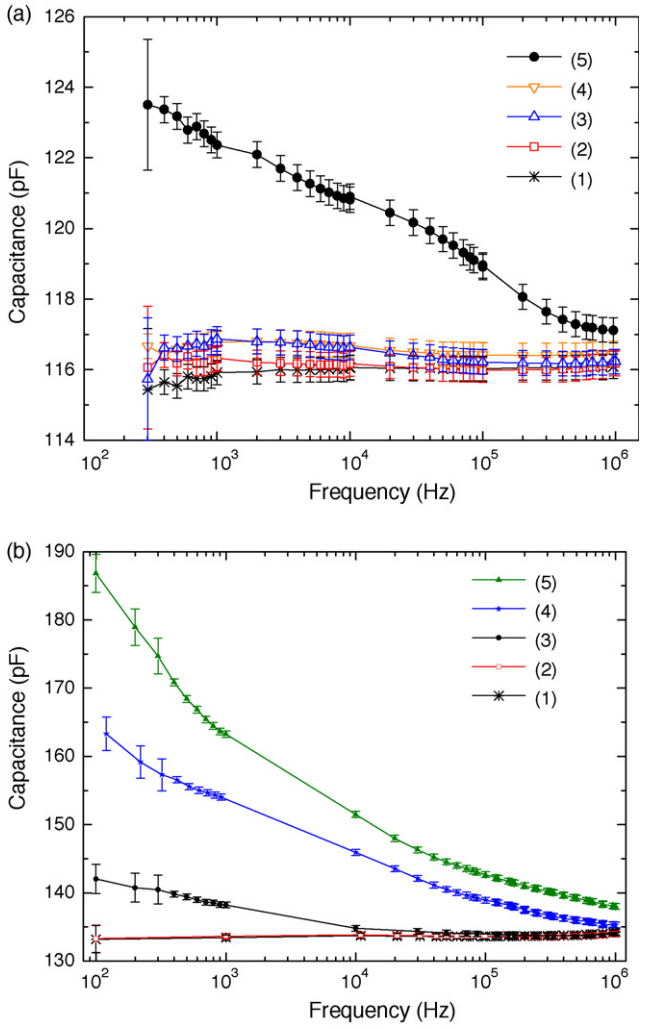

Fig. 3. (a) Device response to IgG. Curve (1): measurement after device fabrication. Curves (2) to (4): measurements after successive pipetting anti-IgG solution onto the electrodes. Curve (5): measurement after IgG solution incubation for 1 h. Curve (5) shows that the antibody–antigen interaction increases the low frequency capacitance. (b) Device response to IgG. Curve (1): measurement after device fabrication. Curve (2): measurement after pipetting of anti-IgG solution onto the electrodes. Curves (3) to (5): measurements after repeated pipetting of IgG solution and incubation for 45 min.

a solution of IgG (1 μg/mL) on the top of the underlying immobilized anti-IgG. The absence of capacitance variation after repeated pipetting of anti-IgG indicated that the surface was completely covered by anti-IgG. After the IgG solution is deposited, device capacitance at lower frequencies increases, as shown in curve (5). In contrast, in Fig. 3(b), the anti-IgG immobilization procedure was performed only once, but the exposure to IgG was repeated. Again, the low-frequency device capacitance was slightly affected by anti-IgG (1 μg/mL) immobilization, but it was greatly affected by the successive deposition of IgG (1 μg/mL) solutions.

The length of the electrodes can vary and correspondingly, the capacitance after device fabrication also varies (the capacitance after antibody immobilization, C_0, is very close to the capacitance after device fabrication). However, the relative capacitance variation is less affected, as shown in Fig. 3(a) and (b). In Fig. 3(a) (curve 4) C_0 (at 300 Hz) is 116.7 pF and the capacitance increases to 123.5 pF (curve 5) after adding 1 μg/mL of IgG. The relative capacitance variation was 5.8%. In Fig. 3(b), another sample with different electrode dimensions has C_0 (at 300 Hz) equal to 133.8 pF (curve 2) and an increase to 140.5 pF (curve 3) after adding 1 μg/mL of

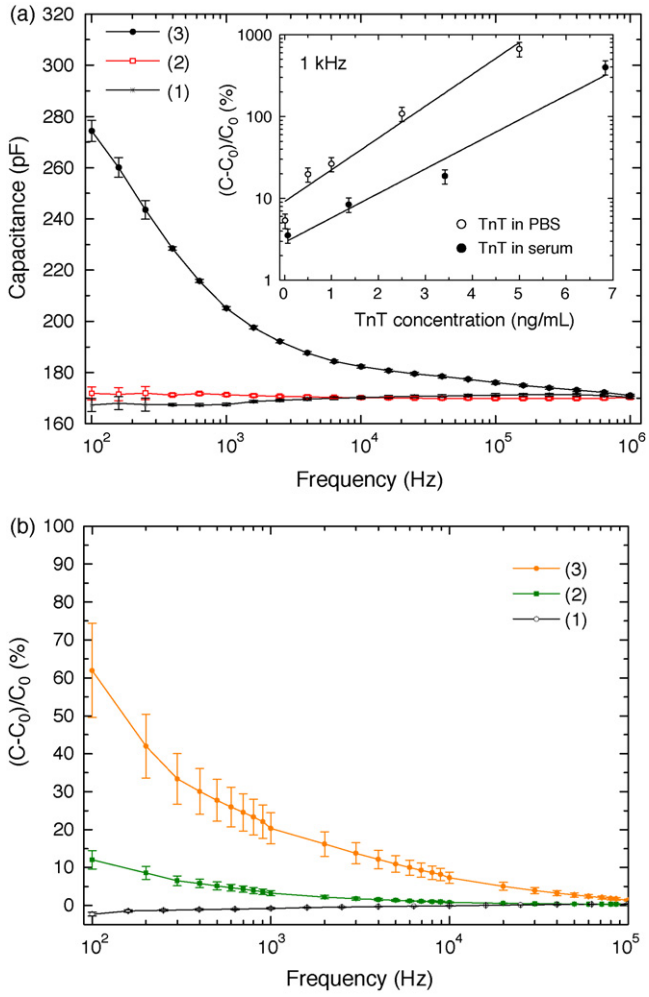

Fig. 4. (a) Device response to TnT. Curve (1): measurement after device fabrication. Curve (2): measurement after pipetting a mixture of anti-TnT + glutaraldehyde (1 ng/mL) and incubation for 1 h followed by DI wash and pipetting glycine solution. Curve (3): measurement after pipetting a solution of anti-TnT in PBS (0.5 ng/mL). Curve (3) shows that the antibody–antigen interaction increases the low frequency capacitance. The inset graph shows relative capacitance changes for different TnT levels in human serum and in PBS solution. Frequency fixed at 1 kHz. (b) Relative capacitance changes when anti-TnT immobilized on the electrodes is exposed to three different antigens. Curve (1): measurement after pipetting non-specific antigen (IgG) in PBS (10 μg/mL) and incubation for 45 min. Curve (2): measurement after pipetting a solution of TnT in PBS (1 ng/mL) that was heated at 50 °C for 30 min. Curve (3): measurement after pipetting a solution of TnT in PBS (1 ng/mL).

IgG. The relative capacitance change was 5.0%. Therefore, C_0 varied 14.7% between samples, whereas the relative capacitance variation differed by only 0.8%.

The increase in the low-frequency device capacitance was also observed when anti-TnT and TnT were used, as shown in Fig. 4(a). It is possible, in principle, to select a fixed, low measurement frequency and calibrate the sensor at such a frequency. This procedure was done when obtaining the data shown in the inset graph of Fig. 4(a). The chosen frequency was 1 kHz, which is a typical measurement frequency in low cost portable capacitance meters.

3.3. Response to troponin T

In order to investigate the feasibility of device calibration for clinical diagnostics, we exposed different devices to different concentrations of TnT. Each device was prepared with an immobilized anti-TnT layer and exposed to a particular antigen concentration, previously measured by the ECLIA method. The inset graph shows the relative capacitance variation measured at 1 kHz for devices exposed to TnT in PBS and exposed to samples of human venous blood serum from patients with cardiac diseases. The cut-off for a cardiac infarction is 0.03 ng/mL (Prasad et al., 2006). For TnT in PBS, we tested from 0.01 ng/mL to 5 ng/mL. The first point of the response to TnT in PBS (inset graph of Fig. 4(a), open symbols) was taken at a TnT concentration of 0.01 ng/mL. So, the biosensor, in principle, is able to detect levels below this threshold. In human serum, we test serum with TnT levels from 0.07 to 6.83 ng/mL that correspond to levels of clinical interest.

Additional evidence of the role played by the antigen–antibody interaction in the low-frequency capacitance increase was obtained from two experiments, whose results are shown in Fig. 4(b). In one experiment, two devices were prepared simultaneously by the anti-TnT immobilization procedure. One of the devices was exposed to a fresh solution of TnT in PBS (1 ng/mL) and the other one was exposed to another portion of the same solution which was kept in a heat bath at 50 °C for 30 min and then cooled to room temperature. It is clear that the relative capacitance variation was reduced for the device whose antigen solution was heated (curve 2) in comparison with the device exposed to the fresh solution (curve 3). This result is consistent with the well known decrease of antibody–antigen affinity constant by exposure to heat (Janeway et al., 2005). Curve 1 shows the result of the other experiment, where we exposed to IgG a device prepared by the anti-TnT immobilization procedure. As expected, the device capacitance did not change, thus indicating good specificity. Overall, the relative standard deviation for the relative capacitance variation in our samples was approximately 20%, which means that reproducibility and calibration are not optimized.

3.4. Equivalent circuit fit for sensor

We developed a preliminary equivalent circuit model that was able to reproduce the general behavior of experimental capacitance versus frequency curves. The circuit is shown in Fig. 5(a). This is our model for the biosensor after immobilization. In this circuit, R_s is the series resistance of the electrodes and C represents the capacitive path between the insulated electrodes through the silicon dioxide layer and silicon substrate and also the fringing capacitance into the air in absence of immobilized layers. R_s and C are always present and are considered constant because the DC bias is kept constant. The effects of the immobilized species are represented by the addition of G_b, C_b and C_{bio}. The capacitance C_b is associated with the insulating layers on the electrodes and the conductance G_b represent charge redistribution and recombination within these layers due to antibody–antigen interaction. C_{bio} is related with fringing capacitance into the air in the presence of the immobilized layers.

The impedance of this circuit is given by:

$$Z_{\text{sensor}} = R_s + 2\frac{\frac{1}{G_b}\times\frac{1}{i\omega C_b}}{\frac{1}{G_b}+\frac{1}{i\omega C_b}} + \frac{\frac{1}{i\omega C}\times\frac{1}{i\omega C_{bio}}}{\frac{1}{i\omega C}+\frac{1}{i\omega C_{bio}}} \quad (2)$$

Simplifying and separating real and imaginary parts:

$$Z_{\text{sensor}} = R_s + \frac{2G_b}{G_b^2 + C_b^2\omega^2} - i\left(\frac{1}{\omega(C+C_{bio})} + \frac{2\omega C_b}{G_b^2 + C_b^2\omega^2}\right) \quad (3)$$

The HP 4284A Precision LCR Meter measures the capacitance and the conductance using a parallel RC circuit model, shown in Fig. 5(b). The impedance of this circuit is given by:

$$Z_{\text{meter}} = \frac{\frac{1}{G}\times\frac{1}{i\omega C_p}}{\frac{1}{G}+\frac{1}{i\omega C_p}} = \frac{1}{G+i\omega C_p} = \frac{G}{G^2+\omega^2 C_p^2} - i\frac{C_p\omega}{G^2+\omega^2 C_p^2} \quad (4)$$

The HP 4284A Precision LCR Meter does not directly measure any of the circuit elements of our biosensor. It measures them indi-

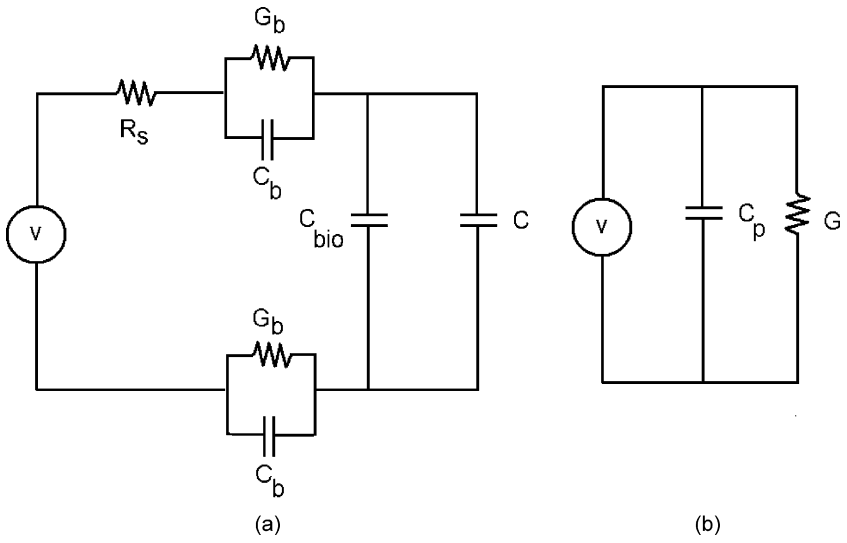

Fig. 5. (a) Biosensor circuit model (b) Equivalent circuit used by the HP 4284A Precision RLC meter. C_p and G are calculated and displayed by the instrument from the measured device current and voltage.

Table 1
Circuit parameters used in the simulations displayed in Fig. 6.

Parameter	Condition		
	Ab	Ag1	Ag2
G_b	5×10^{-10} S	9.5×10^{-7} S	7×10^{-6} S
R_s	0.5 Ω	0.5 Ω	0.5 Ω
C	133 pF	133 pF	133 pF
C_b	2000 pF	2100 pF	2150 pF
C_{bio}	20 pF	20 pF	20 pF

rectly, by means of the C_p and G of a parallel RC circuit. In order to simulate and understand the effect of immobilized species on G_b, C_b and C_{bio} and the corresponding variations on the measured C_p, we have to find an expression relating C_p and the circuit elements of our biosensor. To find this expression, we first compare the real and imaginary parts of Z_{sensor} and Z_{meter} to obtain a system of two equations:

$$R_s + \frac{2G_b}{G_b^2 + C_b^2\omega^2} = \frac{G}{G^2 + \omega^2 C_p^2} \tag{5}$$

$$\frac{1}{\omega(C + C_{bio})} + \frac{2\omega C_b}{G_b^2 + C_b^2\omega^2} = \frac{C_p\omega}{G^2 + \omega^2 C_p^2} \tag{6}$$

Eliminating G by substitution from these two equations, we obtained another equation, where only C_p and the sensor circuit elements appear:

$$C_p R_s^2 + \frac{4C_p R_s G_b}{G_b^2 + C_b^2\omega^2} = \frac{2C_b}{G_b^2 + C_b^2\omega^2} - \frac{4C_p C_b}{(C + C_{bio})(G_b^2 + C_b^2\omega^2)} + \frac{1}{\omega^2(C + C_{bio})} - \frac{1}{\omega^2(C + C_{bio})^2} - \frac{4C_p}{G_b^2 + C_b^2\omega^2} \tag{7}$$

It is now possible to solve this equation for C_p and obtain an expression relating the measured capacitance (C_p) and the biosensor circuit elements (R_s, C, G_b, C_b and C_{bio}):

$$C_p = \frac{(C + C_{bio})[G_b^2 + C_b(2C + C_b + 2C_{bio})\omega^2]}{C_b^2(C + C_{bio})^2 R_s^2\omega^4 + (2C + C_b + 2C_{bio})^2\omega^2 + (C + C_{bio})^2 G_b^2 R_s(4 + G_b R_s)\omega^2 + G_b^2} \tag{8}$$

Fig. 6 shows simulated C_p versus frequency plot with calculated capacitance values with a behavior similar to the experimental

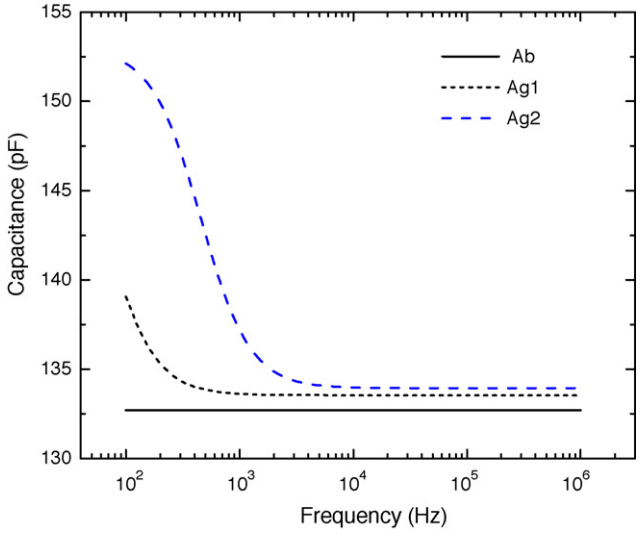

Fig. 6. Calculated parallel capacitance (C_p) versus frequency plot for the biosensor equivalent circuit model when the parameters shown in Table 1 are used.

data shown in Fig. 3(b). Curves in Fig. 6 were calculated using the parameters shown in Table 1. Previous to immobilization, when the electrodes are not covered, our sensor can be considered a simple series RC circuit with a low series resistance. The measured $C_p \times f$ plot is constant, as expected, and the measured C_p values are very close to C if the series resistance is small. Condition antibody (Ab) simulates the sensor after antibody immobilization. A constant $C_p \times f$ plot with the C_p value equal to the geometrical capacitance is also obtained, despite the presence of G_b, C_b and C_{bio}. Conditions antigen 1 (Ag1) and antigen 2 (Ag2) simulate the sensor exposed to two different values of antigen concentration. All parameters, except G_b, did not change much. It is clear that the increase in the conductance G_b resulted in the increased C_p at low frequencies. From the simu-

lations, we conclude that the sensor response is related to changes in G_b, C_b and $C_{bio,}$ with the variations in G_b having most impact. Despite its simplicity and preliminary nature, the equivalent circuit shown in Fig. 5(a) is able to reproduce the general behavior of experimental C_p versus frequency curves. Obviously, more complex circuits, with additional elements will provide a better adjustment to the fine details of the sensor response.

Finally, some points may be emphasized about the practical use of this device. We used very simple device structure and manual pipette dropping methods. This is an innovative test regarding the detection principle, the feasibility of device fabrication and operation at low frequency (1 kHz) permitting the measurement signal in low cost portable capacitance meters. Optimization to build a successful commercial biosensor based on this detection principle may involve sophisticated device structure, including microfluidics techniques for precise deposition of samples.

4. Conclusions

The increase of low frequency capacitance between two planar Al electrodes was used to monitor antibody–antigen interaction. The device detected successfully TnT levels in the range 0.07 ng/mL to 6.83 ng/mL in human blood serum and in the range 0.01 ng/mL to 5 ng/mL for TnT in phosphate buffer saline. An equivalent circuit model able to reproduce the general behavior of experimental capacitance versus frequency curves was presented. The device has potential for the fabrication of a low cost label-free capacitive biosensor. Optimization to build a successful commercial biosensor based on this detection principle may involve improved device structure including microfluidic techniques for precise deposition of the reacting antibody and antigen solutions

Acknowledgments

The authors thank the CNPq and FACEPE (Brazilian agencies) for financial support.

References

Alpert, J.S., Thygesen, K., Antman, E., Bassand, J.P., et al., 2000. Journal of the American College of Cardiology 36 (3), 959–969.
Bangar, M.A., Shirale, D.J., Chen, W., Myung, N.V., Mulchandani, A., 2009. Analytical Chemistry 81 (6), 2168–2175.
Batalla, P., Fuentes, M., Mateo, C., Grazu, V., Fernandez-Lafuente, R., Guisan, J.M., 2008. Biomacromolecules 9, 2230–2236.
Boozer, C., Kim, G., Cong, S., Guan, H., Londergan, T., 2006. Current Opinion in Biotechnology 17 (4), 400–405.
Collinson, P., Gaze, D., 2005. Critical Care 9 (4), 345–346.
Dutra, R.F., Kubota, L.T., 2007. Clinica Chimica Acta 376, 114–120.
Dutra, R.F., Mendes, R.K., Lins, D.A., Silva, V., Kubota, L.T., 2007. Journal of Pharmaceutical and Biomedical Analysis 43 (5), 1744–1750.
Fan, X., White, I.M., Shopova, S.I., Zhu, H., Suter, J.D., Sun, Y., 2008. Analytical Chimica Acta 620 (1–2), 8–26.
Janeway Jr., C.A., Travers, P., Walport, M., Shlomchik, M., 2005. Immunobiology, 6th ed. Garland Science Publishing, New York.
Janshoff, A., Steinem, C., 2005. Methods in Molecular Biology 305, 47–64.
Liu, Y.-C., Wang, C.-M., Hsiung, K.-P., 2001. Analytical Biochemistry 299 (2), 130–135.
Khan, R., Dhayal, M., 2009. Biosensors and Bioelectronics 24 (6), 1700–1705.
Ko, S., Park, T.J., Kim, H.S., Kim, J.H., Cho, Y.J., 2009. Biosensors and Bioelectronics 24 (8), 2592–2597.
Luppa, P.L., Sokoll, L.J., Chan, D.W., 2001. Clinica Chimica Acta 314 (1–2), 1–26.
Prasad, A., Singh, M., Lerman, A., Lennon, R.J., Holmes Jr, D.R., Rihal, C.S., 2006. Journal of the American College of Cardiology 48 (9), 1765–1770.
Qu, L., Xia, S., Bian, C., Sun, J., Han, J., 2009. Biosensors and Biolectronics 24 (12), 3419–3424.
Shiau, A.K., Massari, M.E., Ozbal, C.C., 2008. Combinatorial Chemistry & High Throughput Screening 11 (3), 231–237.
Steen, H., Giannitsis, E., Futterer, S., Merten, C., Juenger, C., Katus, H.A., 2006. Journal of the American College of Cardiology 48 (11), 2192–2194.
Yang, L., Bashir, R., 2008. Biotechnology Advances 26 (2), 135–150.